Available online at www.sciencedirect.com
ScienceDirect
Trans. Nonferrous Met. Soc. China 34(2024) 1237−1250
Transactions of Nonferrous Metals Society of China
www.tnmsc.cn

Oxidation resistance and thermal insulation performance of Al−Cr−O/Zr−O + NiCoCrAlSiY and Al−Cr−O + NiCoCrAlSiY coatings prepared by arc ion plating

Li-jun XIAN[1,2], Hai-bo ZHAO[2], Hong-yuan FAN[1], Guang XIAN[1]

1. School of Mechanical Engineering, Sichuan University, Chengdu 610065, China;
2. Analysis and Testing Centre, Sichuan University, Chengdu 610065, China

Received 14 September 2022; accepted 21 March 2023

Abstract: Al−Cr−O/Zr−O multilayer coating + NiCoCrAlSiY bond layer and Al−Cr−O single-layer coating + NiCoCrAlSiY bond layer were deposited on superalloy by arc ion plating, and subsequently they were heat treated at 1000−1200 °C. Scanning electron microscope and X-ray diffractometer were used to analyze the microstructure and phase of the coatings. The results showed that both the Al−Cr−O/Zr−O multilayer coating and Al−Cr−O single-layer coating exhibited a compact spherical structure. After heat treatment, cracks occurred on the surface of Al−Cr−O/Zr−O coating. Cracks increased and widened with rising the temperature. However, the surface cell clusters of Al−Cr−O coating after heat treatment were changed to tightly connected granular structures, and the granular structures grew up significantly with the increase of annealing temperature. Owing to the oxygen ion conductor and lower densification of t-ZrO_2 than α-Al_2O_3, t-ZrO_2 in the Al−Cr−O/Zr−O coating provided an access for the inward diffusion of oxygen. Therefore, the high temperature oxidation resistance of the Al−Cr−O coating + NiCoCrAlSiY layer was superior to that of the Al−Cr−O/Zr−O multilayer coating + NiCoCrAlSiY layer. The thermal insulation performance of Al−Cr−O/Zr−O multilayer coating + NiCoCrAlSiY layer was better than that of Al−Cr−O coating + NiCoCrAlSiY layer due to the large thickness and low thermal conductivity of t-ZrO_2 phase and the heat reflection of interlayer interface.
Key words: arc ion plating; Al−Cr−O/Zr−O multilayer coating; oxidation resistance; thermal insulation performance

1 Introduction

In order to improve the thrust-to-mass ratio of the engine and the turbine inlet temperature, ZrO_2 based ceramic coatings are widely used in the blades of aero engines and gas turbines to provide high temperature protection for the blades [1−3]. A lot of research has been done on these coatings to further improve the performance [4−7]. High temperature protective coating generally includes a top ceramic coating and a bonding layer [8]. The top ceramic coating plays a dominant role in thermal insulation, reducing the working temperature of the substrate. The bonding layer regulates the thermal expansion coefficient difference in thermal expansion coefficient between top ceramic coating and superalloy substrate, making the coating and substrate more physically compatible. According to different application requirements, high temperature protective coatings can be generally classified into three structural forms: double-layer system, multilayer system and gradient layer system [9−11]. The multilayer system refers to the addition of a barrier layer on the basis of double layers to prevent oxygen and other external corrosive media from entering the bonding layer, thereby delaying the oxidation of the bonding

Corresponding author: Guang XIAN, Tel: +86-13678049163, E-mail: xianguang2014@scu.edu.cn
DOI: 10.1016/S1003-6326(24)66467-8

layer. However, the preparation process of this system is more complicated and its reliability is slightly worse. Gradient layer system refers to a coating whose chemical composition, structure and mechanical properties change continuously along the thickness direction of the coating, so as to avoid premature spalling of the ceramic layer due to excessive thermal stress. But its preparation process is also complicated. Therefore, the double-layer high temperature protective coating is most widely used.

The common preparation methods of high temperature protective coatings include plasma spraying and electron beam physical vapor deposition (EB-PVD). The main advantages of plasma spraying are simple preparation process, high deposition rate and low cost. The disadvantages of plasma spraying are low surface roughness, high porosity and many cracks. These shortcomings aggravate the high temperature oxidation of the coating and get the bonding force between coating and substrate worse [12,13]. Compared with plasma spraying, the coating surface prepared by EB-PVD is more compact, which improves the high temperature oxidation resistance and corrosion resistance. However, the crystalline columnar structure makes the thermal conductivity higher than that of the coating prepared by plasma spraying. In addition, in the preparation process of EB-PVD, it is so difficult to control the composition of the material that the utilization rate of raw material is low [14,15]. Moreover, the high temperature protective coatings deposited through these two coating technologies are usually quite thick (about 150−300 μm). According to Refs. [16−18], the thick ceramic layer has a better high temperature protective effect. However, great stress is induced at the interface between the ceramic layer and the bonding layer when the coating is too thick. It is worth noting that great stress accumulation results in the coating spallation, and then the high temperature protective coating fails [19].

To design an effective thin ceramic coating is one of the most important means to improve the performance and work life of high temperature protective coating. In this study, a thin Al−Cr−O/Zr−O multilayer coating and a thin Al−Cr−O single-layer coating with NiCoCrAlSiY bond layer were deposited by arc ion plating (AIP), respectively. The microstructure, adhesion, high temperature oxidation resistance and thermal insulation performance of the two coatings were systematically investigated.

2 Experimental

2.1 Coating deposition

Al−Cr−O/Zr−O multilayer coating and Al−Cr−O single-layer coating with NiCoCrAlSiY bond layer were deposited on nickel-based superalloy and cemented carbide substrate by AIP, respectively. Cemented carbide substrate was used to prepare fresh fracture specimens for coatings. Superalloy substrate was used for high temperature oxidation experiments and heat insulation experiments. Superalloy was also the application object of ceramic thermal insulation coating. The cleaned and dried substrates were put into the coating chamber, and then the vacuum system was started to evacuate air from the coating chamber. When the back vacuum reached 3.5×10^{-3} Pa, argon gas was introduced into the coating chamber. The substrates revolving in the coating chamber were heated by electron beam and auxiliary heating source. When the substrate temperature reached 400 °C, hydrogen was introduced into the coating chamber. The total pressure in the coating chamber was 0.2 Pa. With a bias of −600 V, the substrate was etched with Ar^+ and H^+ for 70 min. Before depositing Al−Cr−O/Zr−O multilayer coating and Al−Cr−O single-layer coating, a NiCoCrAlSiY (52.2 at.% Ni, 17.5 at.% Co, 23.6 at.% Cr, 6.2 at.% Al, 0.4 at.% Si and 0.1 at.% Y) bonding layer was deposited for 16 h with two NiCoCrAlSiY targets. The deposition was performed in a pure argon atmosphere with the pressure of 9 Pa. The target current was 100 A. The working temperature was 400 °C and the substrate bias voltage was −400 V. The substrates revolved in the chamber with a revolution rate of 1 r/min. This bonding layer could not only improve the bonding strength of the top ceramic coating, but also have good oxidation resistance. Subsequently, $Al_{95}Cr_5$ and Zr targets were used to deposit the Al−Cr−O/Zr−O multilayer coating for 1 h. The $Al_{95}Cr_5$ targets and the Zr targets were placed vertically, as shown in Fig. 1. The working currents of both $Al_{95}Cr_5$ targets and Zr targets were 100 A. During preparing

Al−Cr−O single-layer coating, only the $Al_{95}Cr_5$ targets were used and the current remained unchanged. The deposition atmosphere was a mixture of oxygen and argon, and the flow ratio of oxygen to argon was 3:5. The total pressure was 2 Pa and the substrate bias voltage was −60 V.

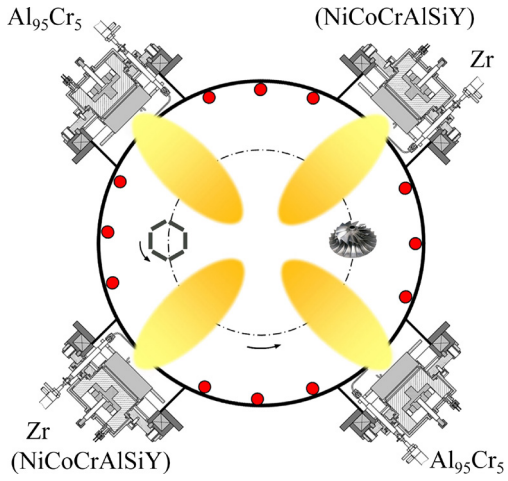

Fig. 1 Schematic diagram of arc ion plating system

2.2 Heat treatment and thermal insulation performance test

The heat treatment was carried out in the SX2−10−12 box-type resistance furnace. Both Al−Cr−O/Zr−O coating + NiCoCrAlSiY layer and Al−Cr−O coating + NiCoCrAlSiY layer were placed in the furnace at room temperature. Subsequently, the furnace temperature rose to 1000, 1100, and 1200 °C in sequence and held for 2 h. For comparison, the uncoated nickel-based superalloy sample was also put into the furnace for heat treatment. The analytical balance (METTLER TOLEDO XS104, and the accuracy of 0.1 mg) was used to weigh the mass of samples before and after oxidation. Mass gain per unit area (ΔG, g/m^2) was calculated by the following formula [9]: $\Delta G=(M_t-M_0)/S$, where M_t is the mass of the sample after heat treatment, M_0 is the mass of the sample before heat treatment, and S is surface area of the sample. The thermal insulation performance tests of the coatings were completed in a self-made test device, as shown in Fig. 2. The coating surface was heated by heat source, and the temperature of coating surface (T_{cs}) was monitored by a thermocouple. Another thermocouple was embedded in the substrate to monitor the temperature of the substrate (T_s). The temperature difference between the coating surface and the substrate was considered as the thermal insulation performance of the coating.

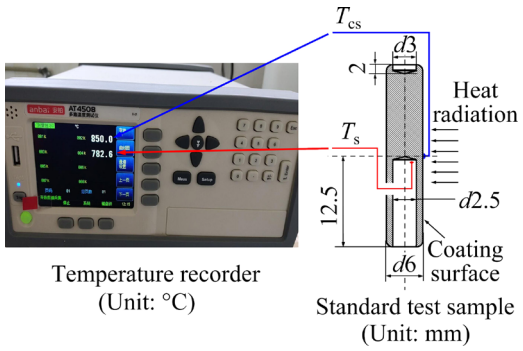

Fig. 2 Schematic diagram of thermal insulation performance test of coatings

2.3 Characterization

Hitachi S4800 scanning electron microscope equipped with the Oxford energy dispersive X-ray spectrometer was used to observe the morphologies and detect the composition of Al−Cr−O/Zr−O coating and Al−Cr−O coating. Bruker D8 Advance X-ray diffraction with Cu K_α (λ=0.15406 nm) X-ray source operating at 40 mA and 40 kV was applied to determining the crystal structure of the coatings. The scanning speed was 2 (°)/min. The scanning step was 0.02° and the scan range was from 30° to 100°. Rockwell indentation test with a load of 150 kg was employed to measure the adhesion between the coating and substrate. The indentation morphology was determined by the scanning electron microscope. In addition, the adhesion strength of the coatings was tested according to the standard of tensile method (ASTM C633 — 01 Standard Test Method for Adhesion or Cohesion Strength of Thermal Spray Coatings).

3 Results and discussion

3.1 Microstructure and composition

Figure 3 shows the cross-sectional morphologies of the Al−Cr−O/Zr−O multilayer coating + NiCoCrAlSiY layer and Al−Cr−O single-layer coating + NiCoCrAlSiY layer. It can be seen from Figs. 3(a, b) that, a coating with about 26.8 μm in thickness was attached to the substrate, which corresponded to the NiCoCrAlSiY bonding layer. There were some fine cracks and pores in the NiCoCrAlSiY bonding layer. The Al−Cr−O/Zr−O

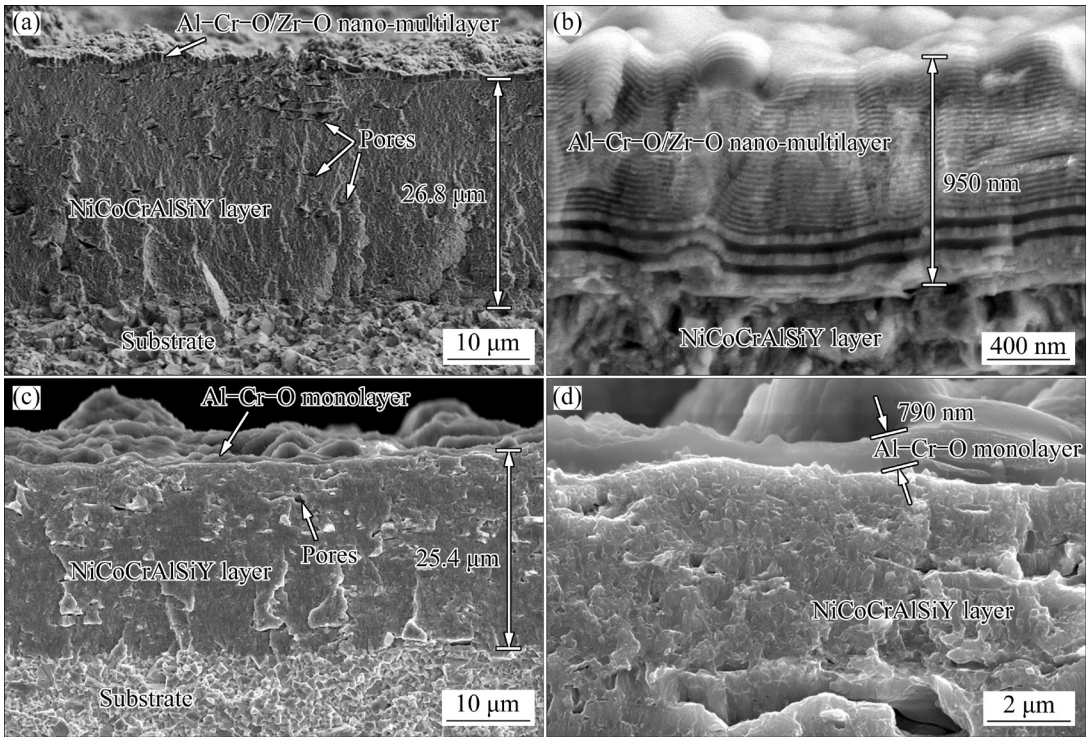

Fig. 3 SEM cross-sectional micrographs of coatings: (a, b) Al−Cr−O/Zr−O multilayer coating + NiCoCrAlSiY bond layer; (c, d) Al−Cr−O single-layer coating + NiCoCrAlSiY bond layer

multilayer coating was 950 nm thick. The interface between the NiCoCrAlSiY bonding layer and the Al−Cr−O/Zr−O coating was obvious. It can be seen from the enlarged morphology of the Al−Cr−O/Zr−O coating that it had a dense laminar structure with alternating nano-layers of Al−Cr−O and Zr−O. The modulation ratio of multilayer coating was about 1:1.2. Obviously, the alternating layers above (about 13 nm) were much thinner than the first four layers below (about 46 nm), which was the result of the poisoning of the $Al_{95}Cr_5$ targets surface during the deposition process and the decrease of deposition rate. The cross-sectional view of Al−Cr−O single-layer coating was shown in Figs. 3(c, d). It can be seen from the enlarged cross-sectional morphology that the thickness of Al−Cr−O coating was 790 nm and thinner than that of Al−Cr−O/Zr−O multilayer coating, because there were only two $Al_{95}Cr_5$ targets working during coating process. The Al−Cr−O coating exhibited a compact structure. Figure 4 shows the surface of the Al−Cr−O/Zr−O multilayer coating and Al−Cr−O single-layer coating. Both the surface of the Al−Cr−O/Zr−O coating and that of Al−Cr−O coating were composed of cellular structure. Small globular cells aggregated to form large cells, and there were small gaps between cellular clusters. The sizes of cellular clusters on the surface of Al−Cr−O/Zr−O coating were larger than those of Al−Cr−O coating.

The compositions of the Al−Cr−O/Zr−O multilayer coating and Al−Cr−O single-layer coating are shown in Fig. 5. According to Fig. 5(a), Al, Cr, Zr and O elements were detected in the Al−Cr−O/Zr−O coating. The oxygen content in the Al−Cr−O/Zr−O coating was about 65 at.%, which was between 60 at.% (atomic percentage of oxygen in Al_2O_3 and Cr_2O_3) and 66.7 at.% (atomic percentage of oxygen in ZrO_2). The Cr/(Al+Cr) ratio was about 28%, which was larger than the original ratio of $Al_{95}Cr_5$ target. This was caused by the higher ionization rate and lower re-sputtering rate of Cr in comparison with Al. Al, Cr and O elements were detected in the Al−Cr−O ceramic coating, as shown in Fig. 5(b). The (Al+Cr)/O ratio was approximately 2:3, which conformed to the stoichiometry of alumina.

Figure 6(a) shows the XRD patterns of the Al−Cr−O/Zr−O multilayer coating + NiCoCrAlSiY layer and Al−Cr−O single-layer coating + NiCoCrAlSiY layer. The diffraction peaks detected in the Al−Cr−O/Zr−O coating mainly corresponded

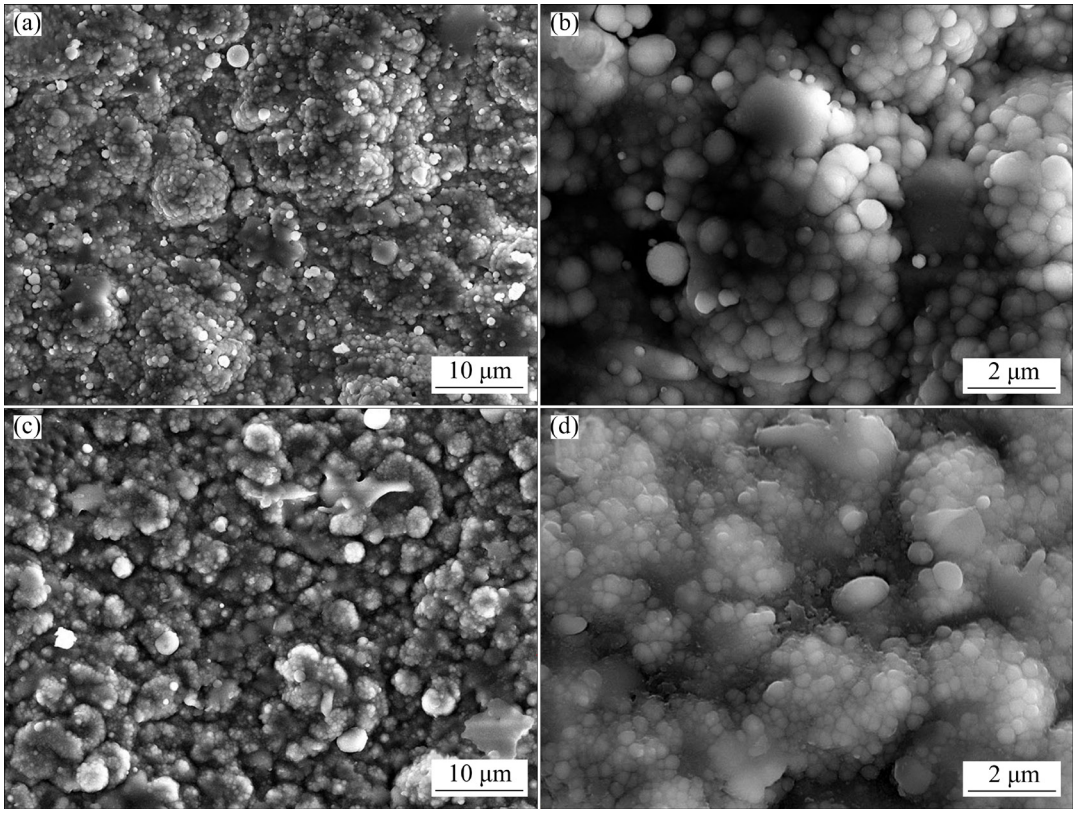

Fig. 4 SEM surface images of coatings: (a, b) Al−Cr−O/Zr−O multilayer coating; (c, d) Al−Cr−O single-layer coating

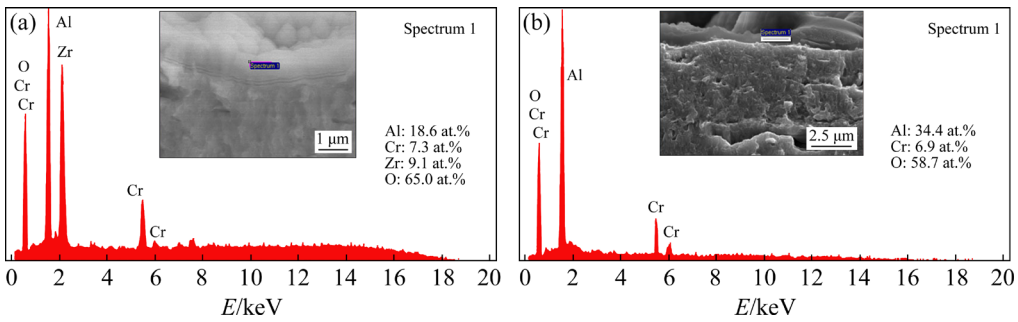

Fig. 5 Chemical composition of coatings: (a) Al−Cr−O/Zr−O multilayer coating; (b) Al−Cr−O single-layer coating

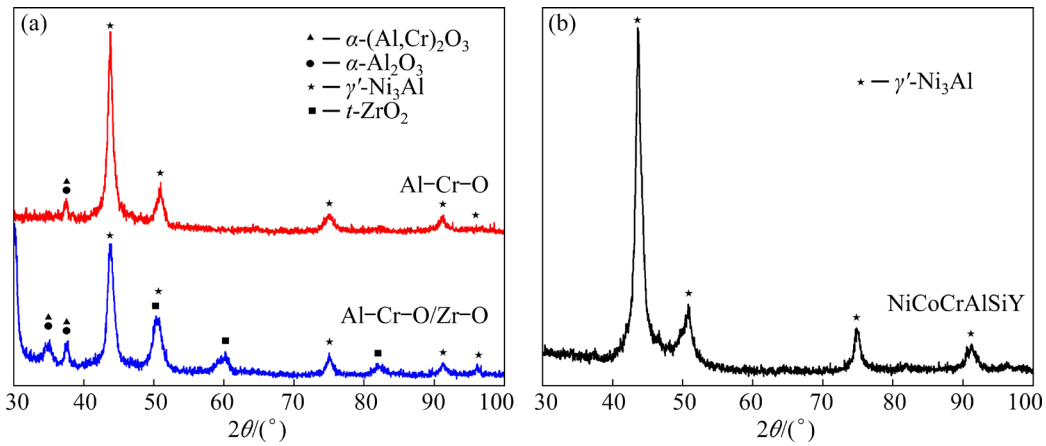

Fig. 6 XRD patterns of Al−Cr−O/Zr−O multilayer coating and Al−Cr−O single-layer coating (a), and NiCoCrAlSiY bond layer (b)

to t-ZrO_2 (JCPDS-ICDD No. 79-1764) phase. In addition, a weak diffraction peak of α-Al_2O_3 (JCPDS-ICDD No. 75-1862) and/or α-$(Al,Cr)_2O_3$ (JCPDS-ICDD No. 71-0958) phase emerged, indicating that the crystallization of alumina was poor. The diffraction peaks of α-Al_2O_3 and α-$(Al,Cr)_2O_3$ were so close that they cannot be distinguished. The strongest diffraction peak in the Al−Cr−O/Zr−O coating + NiCoCrAlSiY layer corresponded to the γ'-Ni_3Al (JCPDS-ICDD No. 09-0097). The top ceramic layer was so thin that the phase of the NiCoCrAlSiY bonding layer was detected, which was in good agreement with the XRD pattern of the NiCoCrAlSiY bonding layer in Fig. 6(b). The diffraction peaks detected in Al−Cr−O coating + NiCoCrAlSiY layer also mainly corresponded to the γ'-Ni_3Al, and the diffraction intensity was stronger than that of the γ'-Ni_3Al in the Al−Cr−O/Zr−O coating. Since the Al−Cr−O coating was thinner than Al−Cr−O/Zr−O coating, it was easier to detect γ'-Ni_3Al phase in the bonding layer. Besides, it was found that the weak diffraction peak of α-Al_2O_3 (and/or α-$(Al,Cr)_2O_3$) phase existed in the Al−Cr−O coating. Therefore, it can be concluded that the multilayer structure and zirconia did not promote the crystallization of alumina.

3.2 Adhesion

Adhesion is a critical measurement of the performance of coating. The Rockwell indentation test was carried out to measure the adhesion of the deposited coatings on superalloy substrate and the results are shown in Fig. 7. According to Refs. [20,21], the indentation can be classified into six levels to characterize the coating's adhesive performance: HF1−HF6. In Fig. 7, only a small number of fine radial cracks were visible in the indentation of Al−Cr−O/Zr−O coating + NiCoCrAlSiY layer and Al−Cr−O coating + NiCoCrAlSiY layer. There was no sign of coating separation or spallation. Therefore, both the indentations of Al−Cr−O/Zr−O coating + NiCoCrAlSiY layer and Al−Cr−O coating + NiCoCrAlSiY layer were deemed to be HF1, which meant that both the Al−Cr−O/Zr−O coating + NiCoCrAlSiY layer and the Al−Cr−O coating + NiCoCrAlSiY layer had excellent adhesion with the superalloy substrate. According to the tensile tests, the adhesion strength of Al−Cr−O/Zr−O coating + NiCoCrAlSiY layer and the Al−Cr−O coating + NiCoCrAlSiY layer deposited on superalloy substrate was (77.7±2.7) MPa and (74.8±3.2) MPa, respectively. The good adhesion can be attributed to the small thermal expansion coefficient difference between the coating and substrate. As given in Ref. [22], the thermal expansion coefficients of the ceramic top layer, the superalloy substrate and the bonding layer NiCoCrAlSiY are $(9-12.2)\times10^{-6}\,K^{-1}$ (25−1100 °C), $(14.8-18)\times10^{-6}\,K^{-1}$ (25−1100 °C) and $(12.3-17.6)\times10^{-6}\,K^{-1}$ (25−1100 °C), respectively. The bonding layer coordinated the thermal expansion coefficients between the ceramic layer and the substrate.

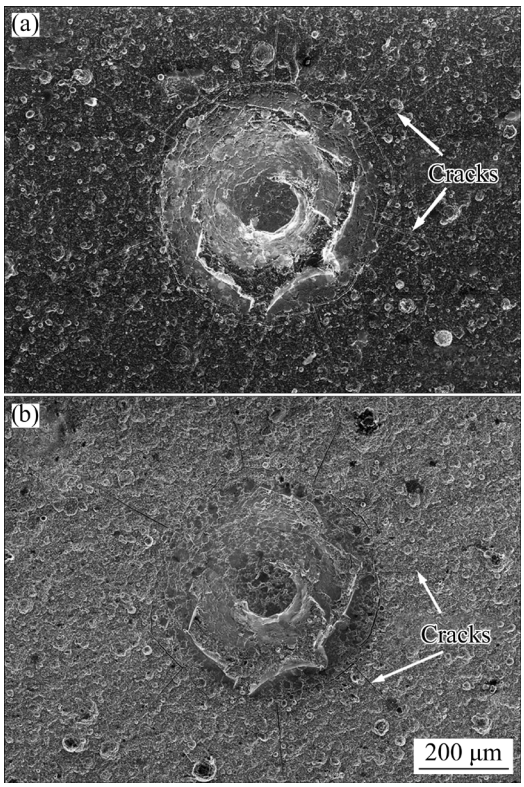

Fig. 7 SEM morphologies of indentation of coatings: (a) Al−Cr−O/Zr−O multilayer coating + NiCoCrAlSiY layer; (b) Al−Cr−O single-layer coating + NiCoCrAlSiY layer

3.3 Oxidation resistance

In order to evaluate the high temperature oxidation resistance of the Al−Cr−O/Zr−O multilayer coating + NiCoCrAlSiY layer and Al−Cr−O single-layer coating+ NiCoCrAlSiY layer, the coated nickel-based superalloy samples were

heat treated at 1000, 1100, and 1200 °C for 2 h, respectively. After heat treatment at 1000 °C, both the Al−Cr−O/Zr−O coating and the Al−Cr−O coating were intact, as shown in Fig. 8. For the NiCoCrAlSiY coated superalloy, a lot of fine discontinuous dark oxides were formed on the surface at 1100 °C heat treatment. When the temperature rose to 1200 °C, the surface oxide grew up significantly. However, the surface of the uncoated superalloy was oxidized and wrinkled obviously at 1000°C. When the heat treatment temperature rose to 1100°C, the oxide scale peeled off. Nevertheless, the Al−Cr−O/Zr−O multilayer coating and Al−Cr−O single-layer coating after annealing at 1200 °C remained intact.

Figure 9 shows the microscopic morphologies of the Al−Cr−O/Zr−O multilayer coating + NiCoCrAlSiY layer and Al−Cr−O single-layer

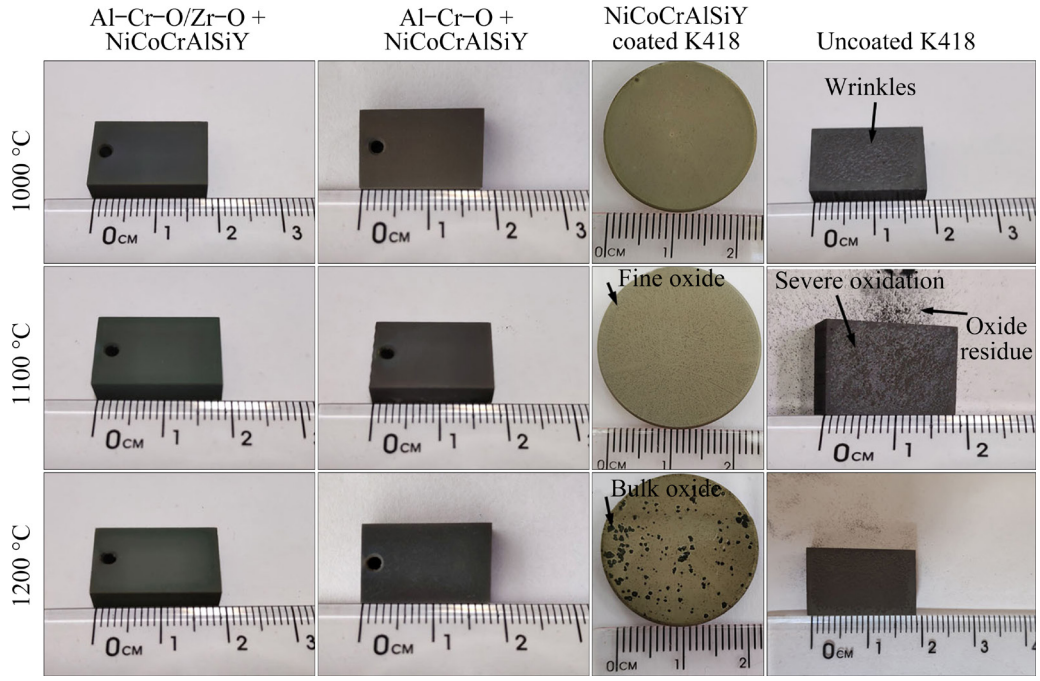

Fig. 8 Appearances of Al−Cr−O/Zr−O + NiCoCrAlSiY, Al−Cr−O + NiCoCrAlSiY, NiCoCrAlSiY coated superalloy as well as uncoated superalloy after heat treatment at 1000−1200 °C

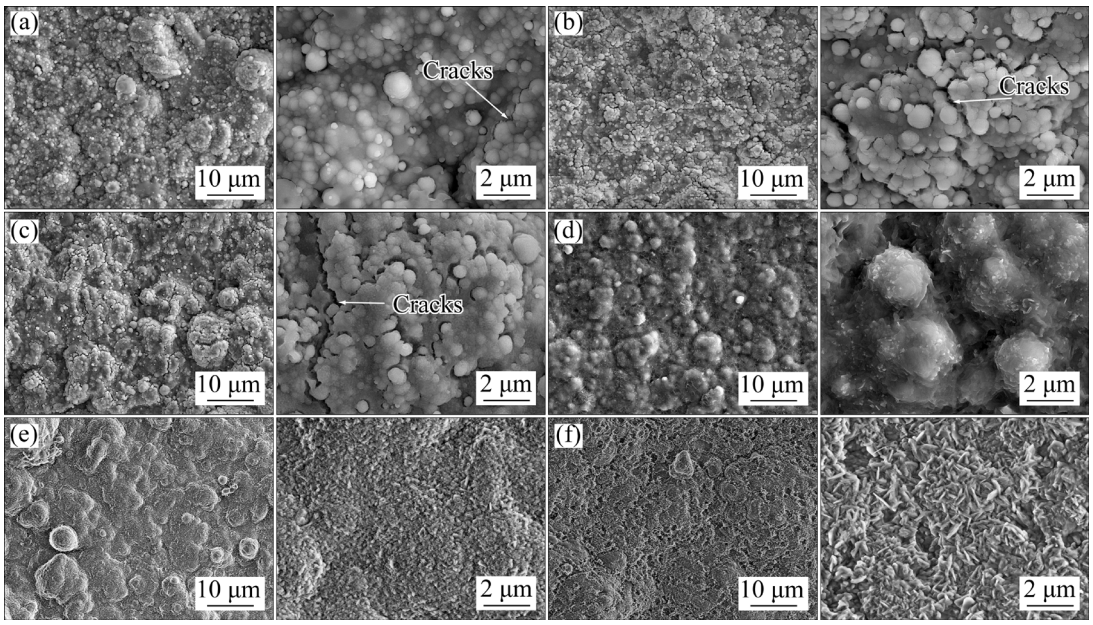

Fig. 9 SEM surface morphologies of coatings after heat treatment: (a) Al−Cr−O/Zr−O, 1000 °C; (b) Al−Cr−O/Zr−O, 1100 °C; (c) Al−Cr−O/Zr−O, 1200 °C; (d) Al−Cr−O, 1000 °C; (e) Al−Cr−O, 1100 °C; (f) Al−Cr−O, 1200 °C

coating + NiCoCrAlSiY layer after heat treatment. It can be seen that the surface of the Al−Cr−O/Zr−O coating + NiCoCrAlSiY layer after heat treatment at 1000 °C was composed of spherical grains, which was the same as the structure of the coating before heat treatment (Fig. 4(a)). The spherical cells did not grow up, but cracks began to sprout among the cellular clusters. When the heat treatment temperature was up to 1100 °C, the number and width of cracks on the coating surface increased. The surface structure of the coating after heat treatment at 1200 °C did not change, which was the same as that after 1100 °C heat treatment. For the Al−Cr−O single-layer coating + NiCoCrAlSiY layer after heat treatment at 1000 °C, the spherical structure of surface became blurred and fine particles grew on the cellular clusters. The surface morphology of Al−Cr−O coating after heat treatment at 1100 °C changed significantly, and the original spherical structure changed into fine particles. In addition, the connection between the particles was dense, filling the gap among the original cellular clusters. Thus, the surface became smoother. After heat treatment at 1200 °C, the grain size of particles on the coating surface grew up obviously and some shallow holes appeared.

The compositions of the Al−Cr−O/Zr−O multilayer coating + NiCoCrAlSiY layer and Al−Cr−O single-layer coating + NiCoCrAlSiY layer after heat treatment are shown in Fig. 10. After heat treatment, the content of Al and O in the Al−Cr−O/Zr−O coating was similar to that before heat treatment. The difference was that the Cr content decreased while Zr content increased for the Al−Cr−O/Zr−O coating after heat treatment. The increase of Zr content in the multilayer coating after oxidation might be caused by the outward diffusion of Zr atoms in the coating. In addition, a small

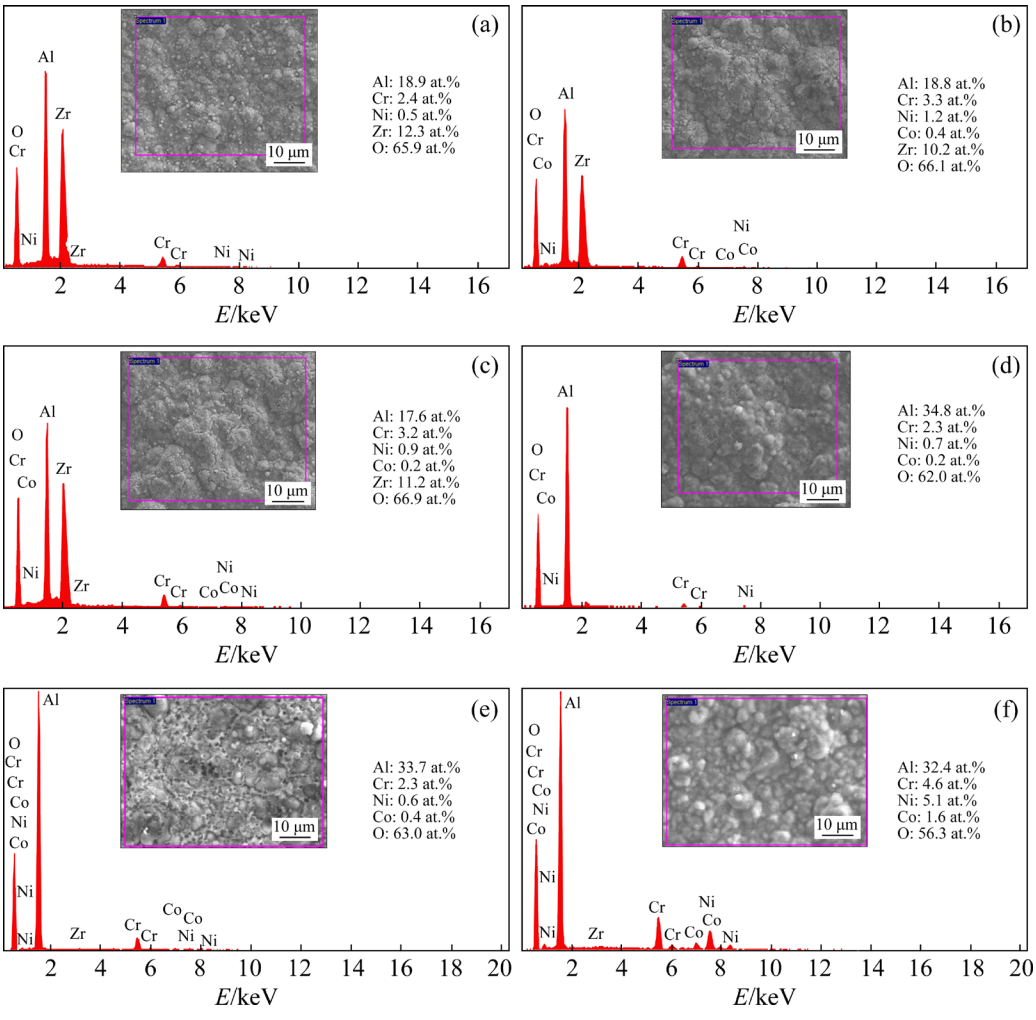

Fig. 10 Chemical compositions of coatings after heat treatment: (a) Al−Cr−O/Zr−O, 1000 °C; (b) Al−Cr−O/Zr−O, 1100 °C; (c) Al−Cr−O/Zr−O, 1200 °C; (d) Al−Cr−O, 1000 °C; (e) Al−Cr−O, 1100 °C; (f) Al−Cr−O, 1200 °C

amount of Ni and Co was detected, which meant that the Ni and Co atoms diffused to the top ceramic coating. The content of Cr in the Al−Cr−O coating after heat treatment was lower than that before heat treatment, and the Al content changed little. A small amount of Ni and Co elements appeared in the top ceramic coating. The content of Ni and Co increased with rising annealing temperature, which meant that more Ni and Co elements diffused into the top coating.

The oxidation mass gain of Al−Cr−O/Zr−O + NiCoCrAlSiY coated, Al−Cr−O + NiCoCrAlSiY coated, NiCoCrAlSiY coated and uncoated samples is shown in Fig. 11. It can be found that the coated samples had less oxidation mass gain than the uncoated superalloy sample, indicating that all the coatings provided a good high temperature protection for the superalloy substrate. Moreover, the oxidation mass gain of Al−Cr−O + NiCoCrAlSiY coated sample was less than that of Al−Cr−O/Zr−O + NiCoCrAlSiY coated sample, suggesting that the oxidation resistance of Al−Cr−O single-layer coating + NiCoCrAlSiY layer was superior to that of Al−Cr−O/Zr−O multilayer coating + NiCoCrAlSiY layer. The oxidation resistance of the merely NiCoCrAlSiY coated sample was similar to that of Al−Cr−O/Zr−O coating + NiCoCrAlSiY coated sample.

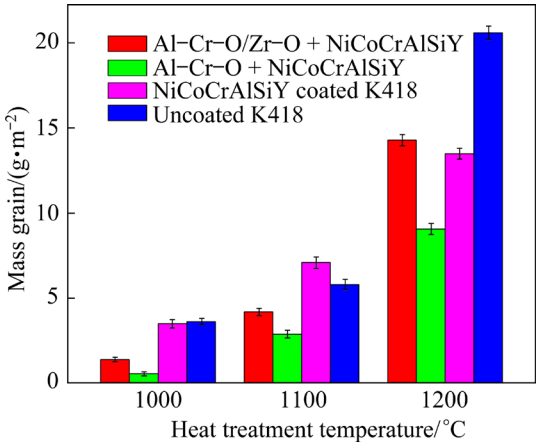

Fig. 11 Mass gain of Al−Cr−O/Zr−O + NiCoCrAlSiY, Al−Cr−O + NiCoCrAlSiY and NiCoCrAlSiY coated superalloy as well as uncoated superalloy after heat treatment at 1000−1200 °C

Figure 12 shows the XRD patterns of the Al−Cr−O/Zr−O multilayer coating + NiCoCrAlSiY layer and Al−Cr−O single-layer coating + NiCoCrAlSiY layer after heat treatment at 1200 °C.

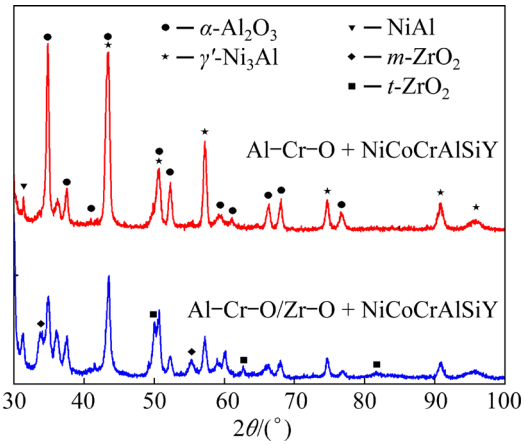

Fig. 12 XRD patterns of Al−Cr−O/Zr−O multilayer coating + NiCoCrAlSiY layer and Al−Cr−O single-layer coating + NiCoCrAlSiY layer after heat treatment at 1200 °C

After high temperature heat treatment, the number and intensity of the diffraction peaks of α-Al_2O_3 in the Al−Cr−O/Zr−O coating + NiCoCrAlSiY layer and Al−Cr−O coating + NiCoCrAlSiY layer increased significantly. At the same time, the intensity of γ'-Ni_3Al diffraction peaks was also enhanced. It was likely that these coatings crystallized at higher temperature. The increase and strengthening of α-Al_2O_3 peaks were partly attributed to the slight oxidation of the inner bonding layer. Besides the diffraction peaks of t-ZrO_2, the diffraction peaks of m-ZrO_2 (JCPDS-ICDD No. 80-0966) were also detected in the Al−Cr−O/Zr−O coating, indicating that the phase transformation of zirconia occurred during the heat treatment, which accounted for the cracks on the surface of the Al−Cr−O/Zr−O coating after heat treatment (Figs. 9(a−c)). Figure 13 shows the cross-sectional micrographs of the Al−Cr−O/Zr−O multilayer coating + NiCoCrAlSiY and Al−Cr−O single-layer coating + NiCoCrAlSiY bond layer after heat treatment at 1200 °C. It could be seen that there were many holes in the two coatings, and the thickness of top oxide coating increased significantly. The composition of different locations in the cross-sectional microstructure of the coatings is given in Table 1. As for the Al−Cr−O/Zr−O multilayer coating + NiCoCrAlSiY layer, the multilayer structure in the top oxide coating disappeared and the oxide layer thickness increased to about 5 μm, which indicated that the inner layer had been oxidized. The oxides were roughly

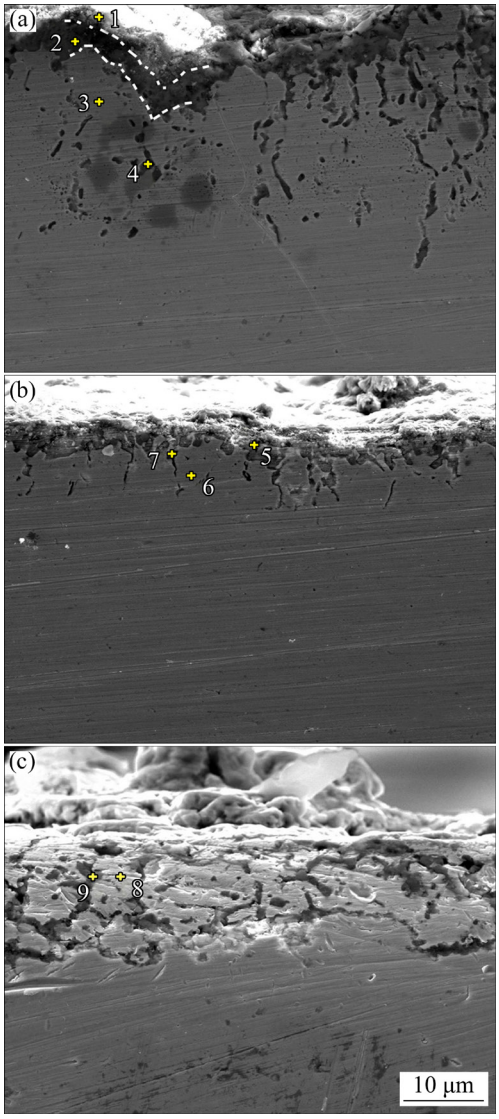

Fig. 13 SEM cross-sectional micrographs of coatings after heat treatment at 1200 °C: (a) Al−Cr−O/Zr−O + NiCoCrAlSiY; (b) Al−Cr−O + NiCoCrAlSiY; (c) NiCoCrAlSiY

Table 1 Compositions at different locations in cross-sectional microstructure shown in Fig. 13 (at.%)

Location No.	O	Al	Cr	Zr	Ni	Co	Si
1	55.5	31.7	5.6	7.2	−	−	−
2	60.7	13.4	25.7	0.2	−	−	−
3	5.4	1.3	22.7	−	52.2	18.4	−
4	50.6	32.3	4.8	−	9.2	3.1	−
5	57.2	35.2	3.9	−	3.7	−	−
6	−	1.9	29.1	−	51.4	17.2	0.4
7	32.7	−	20.5	−	39.1	7.7	−
8	4.8	3.5	21.3	−	53.9	16.5	−
9	54.9	23.4	3.4	−	14.8	3.2	0.3

composed of two layers. The outer oxide layer was loose and rich in Al_2O_3 and ZrO_2 (Location 1) while the inner oxide layer was denser and rich in Cr_2O_3 (Location 2). The content of Al element in the NiCoCrAlSiY bonding layer at Location 3 was significantly lower than that before oxidation, indicating that the Al atoms in the bonding layer diffused outward during high-temperature oxidation. There were a lot of O atoms found in the gray black holes in the bonding layer (Location 4), inferring that these positions had been oxidized by diffused oxygen atoms. According to Fig. 3(a), the pores in the bonding layer provided channels for oxygen atoms, so the oxidation was optimized at these locations. Referring to the Al−Cr−O coating + NiCoCrAlSiY layer, its oxide layer was mainly composed of Al_2O_3 (Location 5) and bonding layer (Location 6) was also poor in Al. In comparison with the depth of holes in Al−Cr−O/Zr−O multilayer coating + NiCoCrAlSiY layer, that of holes formed in the bonding layer for Al−Cr−O coating + NiCoCrAlSiY layer was within 10 μm, indicating that the oxygen atom did not diffuse to the bottom of the bonding layer. Moreover, the average size of the holes in the bonding layer for Al−Cr−O coating + NiCoCrAlSiY layer was smaller. For merely NiCoCrAlSiY coated sample, a lot of aluminum oxide (Location 9) was also formed. The area around the aluminum oxide (Location 8) was poor in aluminum. The depth of oxide formation in the NiCoCrAlSiY layer was similar to that of Al−Cr−O/Zr−O multilayer coating + NiCoCrAlSiY layer, showing that the oxidation resistance of these two coatings was almost equivalent. This result was consistent with the result of oxidation mass gain.

The high temperature protection effect of Al−Cr−O single-layer coating + NiCoCrAlSiY layer was better than that of Al−Cr−O/Zr−O multilayer coating + NiCoCrAlSiY layer due to the superior high temperature oxidation resistance [23,24]. The XRD pattern of Al−Cr−O coating + NiCoCrAlSiY layer before heat treatment showed that, in addition to the γ'-Ni_3Al of the bonding layer, α-Al_2O_3 phase of the ceramic layer was observed. The α-Al_2O_3 phase with the characteristics of dense structure, high stability and low oxygen diffusivity inhibited the penetration of oxygen into the bonding layer effectively [25−27].

Accordingly, oxidation of the bonding layer was delayed. As for the Al−Cr−O/Zr−O coating + NiCoCrAlSiY layer, a large amount of t-ZrO_2 modulation layer was alternately stacked with α-Al_2O_3 layer. According to Ref. [10], t-ZrO_2 provided a channel for the diffusion of oxygen that deteriorated the oxidation resistance of the coating. The density of α-Al_2O_3 crystal and t-ZrO_2 crystal could be calculated respectively by the formula: $K=(\sum n_i \cdot v_i)/V$, where n_i refers to the number of i atom in the unit cell of crystal, v_i refers to the volume of i atom and V is the unit cell volume of crystal. The relative densities of α-Al_2O_3 and t-ZrO_2 were calculated to be 0.70 and 0.54, respectively, which showed that α-Al_2O_3 was denser than t-ZrO_2. In terms of the density of the lattice, t-ZrO_2 was less efficient in preventing oxygen from entering than α-Al_2O_3 did. In addition, the cracks formed on the surface of Al−Cr−O/Zr−O coating after heat treatment destroyed the continuity of the coating and provided a channel for oxygen atoms to enter the coating. Therefore, the Al−Cr−O single-layer coating + NiCoCrAlSiY layer had better high temperature oxidation resistance than the Al−Cr−O/Zr−O multilayer coating + NiCoCrAlSiY layer.

3.4 Thermal insulation performance

Figure 14 shows the temperature of the coating surface and the substrate as a function of heating time. It could be seen from Fig. 14(a) that after 100 min heating, the surface temperature of Al−Cr−O/Zr−O multilayer coating + NiCoCrAlSiY layer reached 850 °C, and then it kept at 850 °C. The temperature of the substrate increased slowly from 770.3 to 784.1 °C with time. Thus, the insulation temperature of the Al−Cr−O/Zr−O multilayer coating + NiCoCrAlSiY layer dropped from 79.7 to 65.9 °C. As shown in Fig. 14(b), when the surface temperature of the Al−Cr−O coating + NiCoCrAlSiY layer reached 850 °C, the corresponding substrate temperature was 798.7 °C. In the subsequent heat preservation process, the substrate temperature increased to 805.7 °C. The insulation temperature of the Al−Cr−O coating + NiCoCrAlSiY layer dropped from 51.3 to 44.3 °C. In addition, the insulation temperature of the NiCoCrAlSiY layer slowly decreased from 21.5 to 13.5 °C during the 850 °C holding process. It could be concluded that the Al−Cr−O/Zr−O coating and the Al−Cr−O coating played an important role in protecting the substrate at high temperature even without the NiCoCrAlSiY layer. It was found by comparison that the Al−Cr−O/Zr−O multilayer coating had a better thermal insulation effect than the Al−Cr−O single-layer coating on account of the comprehensive effect of greater coating thickness,

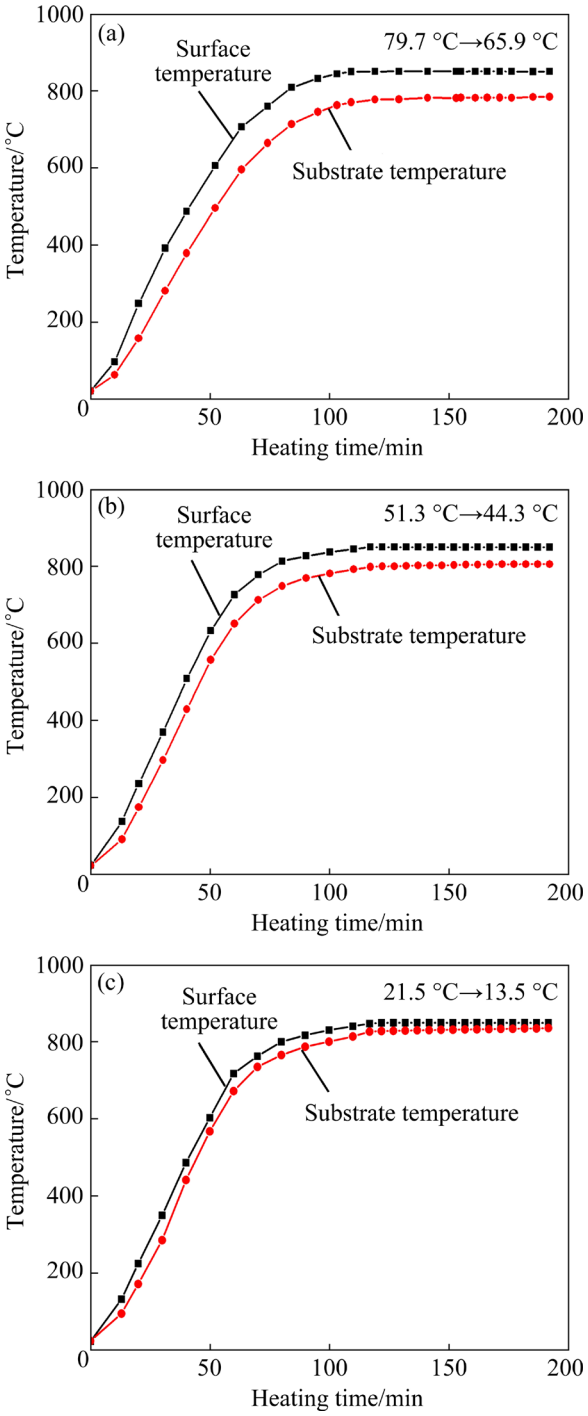

Fig. 14 Insulation temperature of coatings at 850 °C: (a) Al−Cr−O/Zr−O + NiCoCrAlSiY; (b) Al−Cr−O + NiCoCrAlSiY; (c) NiCoCrAlSiY

low thermal conductivity of t-ZrO_2 coating and heat reflection of coating interface.

The superior thermal insulation effect of the Al−Cr−O/Zr−O multilayer coating + NiCoCrAlSiY layer can be explained by the thermal conductivity which is considered to be one of the most important properties of high temperature protective coatings. The content of α-Al_2O_3 in Al−Cr−O coating was higher than that in Al−Cr−O/Zr−O coating. According to Ref. [28], the thermal conductivity of α-Al_2O_3 was 30 $W\cdot m^{-1}\cdot K^{-1}$. However, in addition to α-Al_2O_3 phase, the Al−Cr−O/Zr−O coating had t'-ZrO_2 phase with a thermal conductivity of 3.3 $W\cdot m^{-1}\cdot K^{-1}$ [29]. Therefore, the thermal insulation effect of the Al−Cr−O/Zr−O coating was better. Moreover, the interface between the layers in the Al−Cr−O/Zr−O coating acted as a thermal barrier, improving the thermal insulation performance [30].

4 Conclusions

(1) The thin Al−Cr−O/Zr−O multilayer coating and Al−Cr−O single-layer coating deposited by arc ion plating had a compact cellular structure. Due to the low deposition temperature of arc ion plating, the crystallization of α-Al_2O_3 phase in the deposited coatings was poor. After high temperature heat treatment, the crystallinity of α-Al_2O_3 was improved.

(2) After heat treatment, a large number of cracks were formed on the surface of the Al−Cr−O/Zr−O coating, which was unfavorable to the oxidation resistance. However, the surface of the Al−Cr−O coating + NiCoCrAlSiY layer after heat treatment was transformed into a compact granular structure, which provided a good barrier for the inward diffusion of oxygen.

(3) The high stability and low oxygen diffusivity of α-Al_2O_3 as well as the higher density of α-Al_2O_3 than that of t-ZrO_2 contributed greatly to the better high-temperature oxidation resistance of the Al−Cr−O coating + NiCoCrAlSiY layer.

(4) Due to the large thickness, low thermal conductivity of t-ZrO_2 and the reflection of heat at interlayer interface, the Al−Cr−O/Zr−O multilayer coating + NiCoCrAlSiY layer possessed better thermal insulation performance than the Al−Cr−O single-layer coating + NiCoCrAlSiY layer.

CRediT authorship contribution statement

Li-jun XIAN: Writing − Original draft, Investigation, Data processing; **Hai-bo ZHAO:** Funding acquisition, Investigation, Methodology, Resources; **Hong-yuan FAN:** Conceptualization, Visualization; **Guang XIAN:** Writing − Review & editing, Validation, Supervision.

Declaration of competing interest

The authors declare that they have no known competing financial interests or personal relationships that could have appeared to influence the work reported in this paper.

Acknowledgments

The authors gratefully acknowledge the financial support of this research by the National Defense Science and Technology Key Laboratory Fund Project, China (No. 6142212180103). The authors would like to thank Ling-zhu YU (National Engineering Research Center for Biomaterials, Sichuan University, China) for help in characterizing SEM.

References

[1] BOBZIN K, BROGELMANN T, KALSCHEUER C, YILDIRIM B, WELTERS M. Correlation of thermal characteristics and microstructure of multilayer electron beam physical vapor deposition thermal barrier coatings [J]. Thin Solid Films, 2020, 707: 138081.

[2] SCHULZ U, LEYENS C, FRITSCHER K, PETERS M, SARUHAN-BRINGS B, LAVIGNE O, DORVAUX J M, POULAIN M, MEVREL R, CALIEZ M. Some recent trends in research and technology of advanced thermal barrier coatings [J]. Aerospace Science and Technology, 2003, 7: 73−80.

[3] LU Z, KIM M S, MYOUNG S W, LEE J H, JUNG Y G, KIM I S, JO C Y. Thermal stability and mechanical properties of thick thermal barrier coatings with vertical type cracks [J]. Transactions of Nonferrous Metals Society of China, 2014, 24: 29−35.

[4] YANG Guan-jun, CHEN Zheng-long, LI Cheng-xin, LI Chang-jiu. Microstructural and mechanical property evolutions of plasma-sprayed YSZ coating during high-temperature exposure: comparison study between 8YSZ and 20YSZ [J]. Journal of Thermal Spray Technology, 2013, 22: 1294−1302.

[5] YANG Ming, ZHU Yong-ping, WANG Xue-ying, WANG Qin, AI Li, ZHAO Li-li, CHU Ying. A novel low thermal conductivity thermal barrier coating at super high temperature [J]. Applied Surface Science, 2019, 497: 143774.

[6] DAROONPARVAR M, YAJID M A M, YUSOF N M, FARAHANY S, HUSSAIN M S, BAKHSHESHI-RAD H R,

VALEFI Z, ABDOLAHI A. Improvement of thermally grown oxide layer in thermal barrier coating systems with nano alumina as third layer [J]. Transactions of Nonferrous Metals Society of China, 2013, 23: 1322−1333.

[7] CLARKE D R, PHILLPOT S R. Thermal barrier coating materials [J]. Materials Today, 2005, 8: 22−29.

[8] VOURDAS N, MARATHONITI E, PANDIS P K, ARGIRUSIS C, SOURKOUNI G, LEGROS C, MIRZA S, STATHOPOULOS V N. Evaluation of $LaAlO_3$ as top coat material for thermal barrier coatings [J]. Transactions of Nonferrous Metals Society of China, 2018, 28: 1582−1592.

[9] DONG Tian-shun, WANG Ran, DI Yue-lan, WANG Hai-dou, LI Guo-lu, LIU Li. High temperature oxidation resistance and thermal growth oxides formation and growth mechanism of double-layer thermal barrier coatings [J]. Journal of Alloys and Compounds, 2019, 798: 773−783.

[10] GAO Jun-guo, HE Ye-dong, WANG De-ren. Fabrication and high temperature oxidation resistance of ZrO_2/Al_2O_3 micro-laminated coatings on stainless steel [J]. Materials Chemistry and Physics, 2010, 123: 731−736.

[11] LIMARGA A M, WIDJAJA S, YIP T H. Mechanical properties and oxidation resistance of plasma-sprayed multilayered Al_2O_3/ZrO_2 thermal barrier coatings [J]. Surface and Coatings Technology, 2005, 197: 93−102.

[12] LU Z, MYOUNG S W, KIM E H, LEE J H, JUNG Y G. Microstructure evolution and thermal durability with coating thickness in APS thermal barrier coatings [J]. Materials Today, 2014, 1: 35−43.

[13] NOURI S, SAHMANI S, ASAYESH M, AGHDAM M M. Microstructural characterization of YSZ-CoNiCrAlY two-layered thermal barrier coating formed on γ-TiAl intermetallic alloy via APS process [J]. Intermetallics, 2020, 118: 106704.

[14] BOINSSONNET G, CHALK C, NICHOLLS J R, BONNET G, PEDRAZA F. Phase stability and thermal insulation of YSZ and erbia-yttria co-doped zirconia EB-PVD thermal barrier coating systems [J]. Surface and Coatings Technology, 2020, 389: 125566.

[15] SHI Duo-qi, SONG Jia-nan, LI Shao-lin, QI Hong-yu, YANG Xiao-guang. Cracking behaviors of EB-PVD thermal barrier coating under temperature gradient [J]. Ceramics International, 2019, 45: 18518−18528.

[16] RATZER-SCHEIBE H J, SCHULZ U, KRELL T. The effect of coating thickness on the thermal conductivity of EB-PVD PYSZ thermal barrier coatings [J]. Surface and Coatings Technology, 2006, 200: 5636−5644.

[17] KHOR K A, GU Y W. Thermal properties of plasma-sprayed functionally graded thermal barrier coatings [J]. Thin Solid Films, 2000, 372: 104−113.

[18] HAN Meng, ZHOU Guo-dong, HUANG Ji-hua, CHEN Shu-hai. Optimization selection of the thermal conductivity of the top ceramic layer in the double-ceramic-layer thermal barrier coatings based on the finite element analysis of thermal insulation [J]. Surface and Coatings Technology, 2014, 240: 320−326.

[19] SHEN Wei, WANG Fu-chi, FAN Qun-bo, MA Zhuang. Lifetime prediction of plasma-sprayed thermal barrier coating systems [J]. Surface and Coatings Technology, 2013, 217: 39−45.

[20] GERTH J, WIKLUND U. The influence of metallic interlayers on the adhesion of PVD TiN coatings on high-speed steel [J]. Wear, 2008, 264: 885−892.

[21] DU Hao, ZHAO Hai-bo, XIONG Ji, XIAN Guang. Effect of interlayers on the structure and properties of TiAlN based coatings on WC-Co cemented carbide substrate [J]. International Journal of Refractory Metals and Hard Materials, 2013, 37: 60−66.

[22] SU Luo-chuan, ZHANG Wei-xu, SUN Yong-le, WANG T J. Effect of TGO creep on top-coat cracking induced by cyclic displacement instability in a thermal barrier coating system [J]. Surface and Coatings Technology, 2014, 254: 410−417.

[23] DONG Tian-shun, WANG Ran, DI Yue-lan, WANG Hai-dou, LI Guo-lu, FU Bin-gao. Mechanism of high temperature oxidation resistance improvement of double-layer thermal barrier coatings (TBCs) by La [J]. Ceramics International, 2019, 45: 9126−9135.

[24] OUYANG Tao-yuan, FANG Xuan-wei, ZHANG Ying, LIU Da-wei, WANG Yan, FENG Shuai-jie, ZHOU Tong, CAI Shui-zhou, SUO Jing-pin. Enhancement of high temperature oxidation resistance and spallation resistance of SiC-self-healing thermal barrier coatings [J]. Surface and Coatings Technology, 2016, 286: 365−375.

[25] DALBAUER V, KOLOZSVARI S, RAMM J, KOLLER C M, MAYRHOFER P H. On the oxidation behavior of cathodic arc evaporated Al−Cr and Al−Cr−O coatings [J]. Vacuum, 2019, 163: 1−9.

[26] NAJAFI H, KARIMI A, DESSARZIN P, MORSTEIN M. Formation of cubic structured $(Al_{1-x}Cr_x)_{2+\delta}O_3$ and its dynamic transition to corundum phase during cathodic arc evaporation [J]. Surface and Coatings Technology, 2013, 214: 46−52.

[27] TORKASHVAND K, POURSAEIDI E, MOHAMMADI M. Effect of TGO thickness on the thermal barrier coatings life under thermal shock and thermal cycle loading [J]. Ceramics International, 2018, 44: 9283−9293.

[28] WU Xin-feng, JIANG Ping-kai, ZHOU Yun, YU Jin-hong, ZHANG Fu-hua, DONG Li-hua, YIN Yan-sheng. Influence of alumina content and thermal treatment on the thermal conductivity of UPE/Al_2O_3 composite [J]. Journal of Applied Polymer Science, 2014, 131: 40528.

[29] DELBRUCKE T, GOUVEA R A, RAUBACH C W, LONGO E, SOUSA V C, TEBCHERANIC S M, KUBASKI E T, MOREIRA M L, JURADO J R, CAVA S. Microstructure and thermal conductivity of porous Al_2O_3−ZrO_2 ceramics [J]. Materials Science Forum, 2015, 820: 268−273.

[30] SHEN Lu-wei, ZHANG Ya-mei, ZHANG Pei-gen, SHI Jin-jie, SUN Zheng-ming. Effect of TiO_2 pigment gradation on the properties of thermal insulation coatings [J]. International Journal of Minerals Metallurgy and Materials, 2016, 23: 1466−1474.

电弧离子镀 Al−Cr−O/Zr−O+NiCoCrAlSiY 和 Al−Cr−O+NiCoCrAlSiY 涂层的抗氧化性和隔热性能

鲜丽君[1,2]，赵海波[2]，范洪远[1]，鲜 广[1]

1. 四川大学 机械工程学院，成都 610065；
2. 四川大学 分析测试中心，成都 610065

摘 要：采用电弧离子镀在高温合金表面沉积 Al−Cr−O/Zr−O 多层涂层和 Al−Cr−O 单层涂层+NiCoCrAlSiY 结合层，并在 1000~1200 ℃下进行热处理。利用扫描电子显微镜和 X 射线衍射仪分析涂层的显微组织和物相结构。结果表明，Al−Cr−O/Zr−O 多层涂层和 Al−Cr−O 单层涂层均呈现出致密的球形结构。热处理后，Al−Cr−O/Zr−O 涂层表面出现裂纹，且裂纹随着温度的升高而增多和变粗。然而， Al−Cr−O 涂层经热处理后其表面胞状结构转变为紧密连接的粒状结构，并且随着热处理温度的升高，粒状结构显著长大。由于作为氧离子导体以及 t-ZrO_2 的致密度低于 α-Al_2O_3，Al−Cr−O/Zr−O 涂层中的 t-ZrO_2 为氧离子向涂层内扩散提供了通道，因此，Al−Cr−O 单层涂层+NiCoCrAlSiY 涂层体系的高温抗氧化性优于 Al−Cr−O/Zr−O 多层涂层+NiCoCrAlSiY 涂层体系。但是，由于更大的陶瓷涂层厚度，t-ZrO_2 相的低热导率以及层间界面的热反射作用，Al−Cr−O/Zr−O 多层涂层+NiCoCrAlSiY 涂层体系的隔热性能优于 Al−Cr−O 单层涂层+NiCoCrAlSiY 涂层体系。

关键词：电弧离子镀；Al−Cr−O/Zr−O 多层涂层；抗氧化性；隔热性能

(Edited by Bing YANG)